



## Article

# Improved Multi-GNSS PPP Partial Ambiguity Resolution Method Based on Two-Step Sorting Criterion

Lin Zhao, Zhiguo Sun, Fuxin Yang <sup>\*</sup>, Xiaosong Liu and Jie Zhang

College of Intelligent Systems Science and Engineering, Harbin Engineering University, Harbin 150001, China; zhaolin@hrbeu.edu.cn (L.Z.); sun\_zhiguo@hrbeu.edu.cn (Z.S.); 351031931@hrbeu.edu.com (X.L.); jiezhang@hrbeu.edu.cn (J.Z.)

\* Correspondence: yangfuxin@hrbeu.edu.cn

**Abstract:** Multi-GNSS PPP partial ambiguity resolution (PAR) can improve the fixing success rate and shorten the time to first fix (TTFF). Ambiguity subset selection based on the bootstrapping success rate sorting criterion (BSSC) is widely used in PPP PAR due to its ease of computation and comprehensive evaluation of the global quality of ambiguity solutions. However, due to the influence of unmodeled errors, such as atmospheric residuals and gross errors, ambiguity parameter estimation will inevitably introduce bias. For ambiguity parameters with bias, their variance will converge incorrectly and will not accurately reflect the estimation accuracy. As a result, the selected ambiguity subset based on the BSSC becomes inaccurate, affecting the fixing success rate and TTFF. Therefore, we proposed an improved multi-GNSS PPP PAR method based on a two-step sorting criterion (TSSC). This method aims to address the influence of inaccurate variance of ambiguity parameters, particularly those with low observation quality, on the ambiguity subset selection based on the BSSC. The ambiguity subset satisfying the preset success rate threshold is selected to reduce the influence of unconverged ambiguity on the TSSC. In the first step of the sorting process, the observations whose elevation angle is below 30° or whose posterior residual falls into the IGG3 model reduction domain are clustered together. The posterior observation weight criterion (POWC) instead of the BSSC is adopted to sort ambiguities to overcome the false convergence of variance of ambiguity parameters. In the second step of the sorting process, the remaining ambiguities with reasonable variances are sorted based on the BSSC. Finally, the bottom ambiguity is removed one by one from the ambiguity subset sorted based on the two-step sorting criterion (TSSC) until the requirements of the ratio test for LAMBDA are met. The static data from 10 MGEX stations over a period of 30 days, along with urban kinematic data, were collected to validate the proposed method. Compared with the PAR based on the BSSC, the static experiments demonstrated a reduction of 8.7% and 16.8% in the TTFF and convergence time, respectively. Additionally, the positioning accuracy in the east, north, and up directions was improved by 20.1%, 17.1%, and 4.67%, respectively. Furthermore, the kinematic experiment revealed that the TTFF and convergence time decreased from 1.65 min and 10.5 min to 1.3 min and 1.8 min, respectively, with higher positioning accuracy.

**Keywords:** multi-GNSS; PPP; partial ambiguity resolution; bootstrapping success rate sorting criterion; posterior observation weight criterion



**Citation:** Zhao, L.; Sun, Z.; Yang, F.; Liu, X.; Zhang, J. Improved Multi-GNSS PPP Partial Ambiguity Resolution Method Based on Two-Step Sorting Criterion. *Remote Sens.* **2023**, *15*, 3319. <https://doi.org/10.3390/rs15133319>

Academic Editors: Chuang Shi, Shengfeng Gu, Yidong Lou, Xiaopeng Gong, Fu Zheng and Xiaomin Luo

Received: 23 May 2023

Revised: 23 June 2023

Accepted: 26 June 2023

Published: 28 June 2023



**Copyright:** © 2023 by the authors. Licensee MDPI, Basel, Switzerland. This article is an open access article distributed under the terms and conditions of the Creative Commons Attribution (CC BY) license (<https://creativecommons.org/licenses/by/4.0/>).

## 1. Introduction

Precise Point Positioning (PPP) is a fundamental technology in the field of global navigation satellite systems (GNSS) precise positioning, offering the advantage of achieving sub-decimeter or even centimeter-level accuracy with a single receiver [1]. However, the long convergence time of float-based PPP affects real-time applications. In comparison, carrier phase integer ambiguity resolution (AR) can reduce convergence time and enhance positioning accuracy [2–4]. However, the full ambiguity resolution (FAR) of PPP typically takes tens of min [5–7]. With the development of the Global Positioning System (GPS),

GLOBAL NAVIGATION Satellite System (GLONASS), BeiDou Navigation Satellite System (BDS), and Galileo, multi-GNSS PPP can improve the convergence time and positioning accuracy due to better spatial geometry and more observations [8–11]. However, multi-GNSS PPP FAR always takes a longer time to first fix (TTFF) and a lower fixing success rate due to the frequent occurrence of low-quality observation satellites [5].

Partial ambiguity resolution (PAR) can enhance the AR success rate and reduce the TTFF [12]. The selection criterion for the ambiguity subset is crucial to reducing the TTFF and improving the fixing success rate of PAR. In order to improve the fixing success rate of AR, Teunissen et al. proposed an ambiguity subset selection method based on the success rate criterion (SRC) [13]. The ambiguity subset is determined when its success rate satisfies the preset success rate threshold (PSRT). Although the SRC can provide a probability of successfully fixing the ambiguity, its fixed solution reliability is difficult to guarantee due to low-quality observation satellites. Mowlam et al. proposed an advanced SRC ambiguity subset selection method combined with an elevation angle [14]. This method iteratively excludes satellites with the lowest elevation angle to make the ambiguity subset meet the PSRT. Additionally, the ratio test is a commonly employed method for assessing the correctness of ambiguity estimation. To further enhance the reliability of the fixed solution, the ratio test is typically conducted following the LAMBDA search [15–18]. Wang et al. proposed a method for selecting ambiguity subsets based on the bootstrapping success rate sorting criterion (BSSC). In this method, the PSRT and ratio test were used to verify the fixed solution to reduce the probability of accepting incorrect fixed solutions [19]. However, the fixing success rate will be limited because the ratio test is only applied to the maximum ambiguity subset, which meets the PSRT, whereas the remaining subsets, which may satisfy the ratio test within the maximum ambiguity subset, are not validated. Li et al. improved the method by removing ambiguities with the lowest bootstrapping success rate until the requirements of both the PSRT and ratio test were met for the sub-subset, which improved the fixing success rate [12]. Therefore, the ambiguity subset selection based on the BSSC is widely used in PPP PAR due to its simple calculation and comprehensive evaluation of the global quality of ambiguity solutions. However, the success rate calculation of bootstrapping assumes that the ambiguities are unbiased—biases consisting of unmodeled errors with low elevation angle atmospheric residuals and gross errors in harsh environments are introduced to the ambiguity parameters. This leads to false convergence for the variance of the biased ambiguity parameters [20,21]. Due to the presence of false convergence in the biased ambiguity parameters, the reliability of the ambiguity subset selection method based on the BSSC is difficult to guarantee, and the performance of multi-GNSS PPP PAR will degrade.

It is well known that unmodeled errors, such as atmospheric residuals and multipath effects, have a greater impact on satellite observations when the elevation angle of the satellite decreases. Currently, most studies divide the stochastic model of observations into two segments with a 30° elevation angle boundary [20,22,23]. It is generally believed that satellites below a 30° elevation angle are significantly affected by atmospheric residuals and multipath effects. When the satellite elevation angle is below 30°, the weight of observations will decrease. Otherwise, the weight values of observations are equal. The posterior observation weight based on the IGG3 model reflects the accuracy of observations more reasonably than the prior observation weight based on the elevation angle stochastic model [24]. Although the robust Kalman filter based on the IGG3 model can mitigate the impact of unmodeled errors to some extent, the false convergence for the variance of the biased ambiguity parameters cannot be completely excluded [25,26]. The Schmidt-Kalman filter (SKF) is the simplest filtering algorithm for stochastic systems which takes into account the uncertainty statistics of parameters but does not update them [27,28]. While the SKF is well known and has been used in covariance analysis, not much attention has been given to its actual implementations in a real-time recursive estimation algorithm.

To mitigate the impact of inaccurate variance of biased ambiguity parameters caused by low-quality observations on the BSSC ambiguity subset selection, we proposed an

improved multi-GNSS PPP PAR method based on the two-step sorting criterion (TSSC). In this contribution, observations under the following two circumstances will be clustered together: the first is observations with an elevation angle below  $30^\circ$ , and the second is the ones whose posterior residual falls into the IGG3 model reduction domain. The posterior observation weight criterion (POWC) instead of the BSSC is adopted to sort ambiguities to overcome the false convergence of variance, and the remaining ambiguities with reasonable variances are sorted based on the BSSC. Finally, a subset of the sorted ambiguities based on TSSC is obtained, and all ambiguities are gradually excluded from the ambiguity subset until the requirements of the ratio test for LAMBDA are met.

The chapters of this paper are arranged as follows. In Section 2, we give a brief introduction to the multi-GNSS PPP AR model. In Section 3, we introduce PPP PAR based on the TSSC process. In Section 4, we validate the effectiveness of the proposed method using static data collected from 10 MGEX stations over a 30-day period, along with urban kinematic data. Finally, we present the discussion and conclusion of our study.

## 2. Multi-GNSS PPP AR Model

For a user receiver  $r$  tracking the satellite  $s$  on frequency  $j$ , the functional model of code and carrier phase observation equations can be formulated as:

$$\begin{cases} P_{r,j}^{s,\text{sys}} = \rho_r^{s,\text{sys}} + M_w^{s,\text{sys}} \cdot Z_w + c \left( dt_r^{s,\text{sys}} - dt^{s,\text{sys}} \right) + I_{r,j}^{s,\text{sys}} + d_{r,j}^{s,\text{sys}} - d_j^{s,\text{sys}} + \varepsilon_{P_{r,j}^{s,\text{sys}}} \\ L_{r,j}^{s,\text{sys}} = \rho_r^{s,\text{sys}} + M_w^{s,\text{sys}} \cdot Z_w + c \left( dt_r^{s,\text{sys}} - dt^{s,\text{sys}} \right) - I_{r,j}^{s,\text{sys}} + \lambda_j \cdot \left( N_{r,j}^{s,\text{sys}} + b_{r,j}^{s,\text{sys}} - b_j^{s,\text{sys}} \right) + \varepsilon_{L_{r,j}^{s,\text{sys}}} \end{cases} \quad (1)$$

The symbols  $P$  and  $L$  denote code and carrier phase observations in meters, respectively, and their noises are  $\varepsilon_P$  and  $\varepsilon_L$  in meters, respectively; sys denotes constellation system;  $\rho$  is the geometric distance between receiver antenna phase center and satellite antenna phase center in meters;  $Z_w$  is the wet part of the tropospheric delay in the zenith direction in meters;  $M_w$  is the mapping function of  $Z_w$ ;  $c$  is the speed of light in meters per second;  $dt$  and  $dt^s$  are, respectively, the receiver clock and satellite clock errors in seconds;  $I$  is the slant ionospheric delay in meters;  $d_r$  and  $d^s$  are the receiver-side and the satellite-side code hardware delay in meters;  $\lambda_j$  is the wavelength of frequency  $j$  in meters/cycles;  $N$  is the undifferenced integer ambiguity in cycles;  $b_r$  is the receiver-side carrier phase hardware delay in cycles;  $b^s$  is the satellite-side carrier phase hardware delay in cycles. In brief, the errors including phase wind-up, dry tropospheric delay, tidal displacements, earth rotation, and relativistic effects can be corrected using existing models [29].

Generally, carrier phase hardware delay bias of the satellite- and receiver-side will be merged into the undifferenced ambiguity. In order to recover the integer characteristic of undifferenced carrier phase ambiguity, the receiver-side hardware delay bias is usually eliminated by the between-satellite single difference (BSSD). The satellite-side hardware delays are generally eliminated by external correction information. In order to meet the needs of PPP AR users under various observation combination modes, IGS proposed observable-specific signal biases (OSBs) based on the SINEX format, which can directly correct the original observations [30,31]. The functional models based on OSBs product correction are shown in the following equation:

$$\begin{cases} \bar{P}_{r,j}^{s,\text{sys}} = P_{r,j}^{s,\text{sys}} - \bar{d}_{j,\text{OSBs}}^{s,\text{sys}} \\ \bar{L}_{r,j}^{s,\text{sys}} = L_{r,j}^{s,\text{sys}} - \bar{b}_{j,\text{OSBs}}^{s,\text{sys}} \end{cases} \quad (2)$$

where  $\bar{d}_{j,\text{OSBs}}^{s,\text{sys}}$  and  $\bar{b}_{j,\text{OSBs}}^{s,\text{sys}}$  are the code and carrier phase OSBs in meters, respectively.

In order to eliminate first-order ionospheric delay, the dual-frequency ionosphere-free (IF) combination observations are as follows:

$$\begin{cases} P_{r,IF}^{s,sys} = \alpha \bar{P}_{r,1}^{s,sys} + \beta \bar{P}_{r,2}^{s,sys} = \rho_r^{s,sys} + M_w^{s,sys} \cdot Z_w + c(dt_r^{sys} - dt^{s,sys}) + d_{r,IF}^{sys} + \varepsilon_{P_{r,IF}^{s,sys}} \\ L_{r,IF}^{s,sys} = \alpha \bar{L}_{r,1}^{s,sys} + \beta \bar{L}_{r,2}^{s,sys} = \rho_r^{s,sys} + M_w^{s,sys} \cdot Z_w + c(dt_r^{sys} - dt^{s,sys}) + \lambda_{IF} (N_{r,IF}^{s,sys} + b_{r,IF}^{sys}) + \varepsilon_{L_{r,IF}^{s,sys}} \end{cases} \quad (3)$$

where the subscripts 1 and 2 represent the corresponding BDS B1I and B3I frequencies, GPS L1 and L2 frequencies, and Galileo E1 and E5a frequencies, respectively;  $\alpha = f_1^2 / (f_1^2 - f_2^2)$  and  $\beta = -f_2^2 / (f_1^2 - f_2^2)$  are IF combination coefficients;  $\lambda_{IF}$  is the wavelength of IF combination in meters/cycles;  $N_{r,IF}^{s,sys}$  is the float IF combination ambiguity in cycles;  $b_{r,IF}^{sys}$  is the carrier phase hardware delay bias of receiver-side in cycles;  $d_{r,IF}^{sys}$  is the code hardware delay bias of receiver-side in meters.

To achieve ambiguity resolution in IF combination PPP, the IF ambiguity is typically divided into wide-lane integer ambiguity and narrow-lane float ambiguity:

$$\hat{N}_{r,IF}^{s,sys} = \frac{\lambda_1}{\lambda_1 + \lambda_2} \hat{N}_{r,nl}^{s,sys} + \frac{\lambda_1^2}{\lambda_2^2 - \lambda_1^2} \overset{\sim}{N}_{r,wl}^{s,sys} \quad (4)$$

where  $\overset{\sim}{N}_{r,wl}^{s,sys}$  denotes wide-lane integer ambiguity in cycles;  $\hat{N}_{r,nl}^{s,sys}$  denotes narrow-lane float ambiguity.

The float wide-lane ambiguity is obtained by Hatch-Melbourne-Wübbena (HMW) combination [32–34]:

$$\lambda_{wl} \cdot \bar{N}_{r,wl}^{s,sys} = \frac{f_1 \cdot \bar{L}_{r,1}^{s,sys} - f_2 \cdot \bar{L}_{r,2}^{s,sys}}{f_1 - f_2} + \frac{f_1 \cdot \bar{P}_{r,1}^{s,sys} + f_2 \cdot \bar{P}_{r,2}^{s,sys}}{f_1 + f_2} = \lambda_{wl} \cdot (N_{r,wl}^{s,sys} + \mu_{r,12}^{sys}) \quad (5)$$

where  $\bar{N}_{r,wl}^{s,sys}$  is the float wide-lane ambiguity in cycles;  $\lambda_{wl} = c / (f_1 - f_2)$  is the wide-line ambiguity wavelength;  $N_{r,wl}^{s,sys}$  is the integer wide-lane ambiguity in cycles;  $\mu_{r,12}^{sys}$  is the HMW combination code and carrier phase hardware biases at receiver in cycles.

In order to recover the integer characteristic of wide-lane ambiguity, the receiver-side hardware delay bias is usually eliminated by the BSSD. The nearest rounding decision function is used to fix the BSSD wide-lane ambiguity [20]. When the BSSD wide-lane ambiguity is successfully fixed, the BSSD narrow-lane ambiguity with integer characteristics can be obtained by Equation (4). The LAMBDA method satisfying the ratio test is used to fix the BSSD narrow-lane ambiguity.

### 3. PPP PAR Method Based on Two-Step Sorting Criterion

#### 3.1. Posterior Observation Weight Criterion

The IGG3 model can suppress abnormal observations by constructing equivalent weight factors. The equivalent weight function is as follows [35]:

$$p_i = \begin{cases} 1 & , \quad |\bar{v}_i| \leq k_0 \\ \frac{k_0}{|\bar{v}_i|} \left( \frac{k_1 - |\bar{v}_i|}{k_1 - k_0} \right)^2 & , \quad k_0 < |\bar{v}_i| < k_1 \\ 0 & , \quad |\bar{v}_i| \geq k_1 \end{cases} \quad (6)$$

where  $p_i$  is the weight reduction factor;  $\bar{v}_i$  is the standardized posterior residual of the code or carrier phase;  $k_0$  and  $k_1$  are constants. In this paper,  $k_0$  takes 1.5 and  $k_1$  takes 3.0. In the IGG3 model, once the satellite code or carrier phase standardized posterior residuals fall into the rejection domain, they will be excluded. If multiple satellites fall into the rejection region at the same time, only the observation with the largest variance is excluded [36]. In order to ensure computational efficiency, the maximum number of iterations is set to 6.

The posterior observation weight matrix based on the IGG3 model can be written as follows:

$$\bar{\mathbf{P}}_{L_k} = \mathbf{P}_{L_k} \mathbf{P}_k, \mathbf{P}_k = \text{diag}(p_i) \quad (7)$$

where  $\mathbf{P}_{L_k}$  is the prior observation weight matrix using elevation angle stochastic model in dimension  $n \times n$ ;  $\bar{\mathbf{P}}_{L_k}$  is the posterior observation weight matrix based on the IGG3 model in dimension  $n \times n$ .

Due to the influence of unmodeled errors, such as atmospheric residuals and gross errors, the variances of ambiguity parameters exist in false convergence, which cannot accurately reflect its estimation accuracy. The POWC is sorted from small to large according to the posterior weight of the carrier phase observation. To avoid the adverse effects of ambiguity variance inaccuracy on the ambiguity subset selection when using the BSSC, the ambiguity subset based on POWC can be determined as follows: (1) The ambiguity subset  $\hat{\mathbf{a}}_m$  that meets the PSRT to reduce the influence of unconverged ambiguities is selected. (2) The ambiguities whose observation elevation angle is below  $30^\circ$  or whose posterior residual falls into the IGG3 model reduction domain are clustered together, denoted as  $\hat{\mathbf{a}}_1$ . The POWC is adopted to sort ambiguities to overcome the false convergence of variance of ambiguity parameters.

### 3.2. Bootstrapping Success Rate Sorting Criterion

Due to the lower bound of the success rate of integer least squares estimation, the success rate of bootstrapping has been proven to be a solution to the success rate of integer least squares with a very high degree of approximation. The success rate of bootstrapping can be calculated as follows [13]:

$$P_{s,B} = \prod_{i=1}^n \left( 2\Phi \left( \frac{1}{2\sigma_{\hat{N}_{i|I}}} \right) - 1 \right) \quad (8)$$

$$\Phi(x) = \frac{1}{\sqrt{2\pi}} \int_{-\infty}^x \exp \left\{ -\frac{1}{2}t^2 \right\} dt \quad (9)$$

where  $\hat{N}_{i|I}$  is the abbreviation of  $\hat{N}_{i|i-1, \dots, 1}$ , which is the conditional estimation of the  $i$ th ambiguity with the previous  $i-1$  ambiguity fixed to the integer;  $\sigma$  is the standard deviation of  $\hat{N}_{i|I}$ ;  $\Phi(x)$  is a normal distribution function.

The BSSC method sorts the ambiguity from small to large according to the bootstrapping success rate of the ambiguity; then, partial ambiguity screening is realized. The remaining subset of ambiguities with reasonable variances except  $\hat{\mathbf{a}}_1$  in  $\hat{\mathbf{a}}_m$  are denoted as  $\hat{\mathbf{a}}_2$ . The  $\hat{\mathbf{a}}_2$  are sorted based on the BSSC.

Combined with the POWC and BSSC, we proposed an improved multi-GNSS PPP PAR method based on TSSC, abbreviated as TSSC-PAR. Figure 1 shows the processing of the TSSC-PAR. The basic process is as follows:

1. Stage 1. The ambiguity subset satisfying the PSRT is selected to reduce the influence of unconverged ambiguity on the TSSC.
2. Stage 2. In the first step of sorting based on TSSC, the POWC method is used to sort the ambiguities in the ambiguities subset  $\hat{\mathbf{a}}_1$ , and the sorted ambiguities subset is denoted as  $\hat{\mathbf{a}}_1^-$ . This process helps avoid selecting inaccurate variance of the ambiguity based on the BSSC method.
3. Stage 3. In the second step of sorting based on TSSC, the BSSC method is used to sort the ambiguities in the ambiguities subset  $\hat{\mathbf{a}}_2$ , and the sorted ambiguities subset is denoted as  $\hat{\mathbf{a}}_2^-$ .  $\hat{\mathbf{a}}_1^-$  and  $\hat{\mathbf{a}}_2^-$  are combined to form  $\hat{\mathbf{a}}_{\bar{m}} = [\hat{\mathbf{a}}_2^- \ \hat{\mathbf{a}}_1^-]^T$ .
4. Stage 4. Finally, the bottom ambiguity from  $\hat{\mathbf{a}}_{\bar{m}}$  is one by one excluded until either the ratio test is met or the number of participating fixed ambiguities falls below 5. Otherwise, the float solution is output.

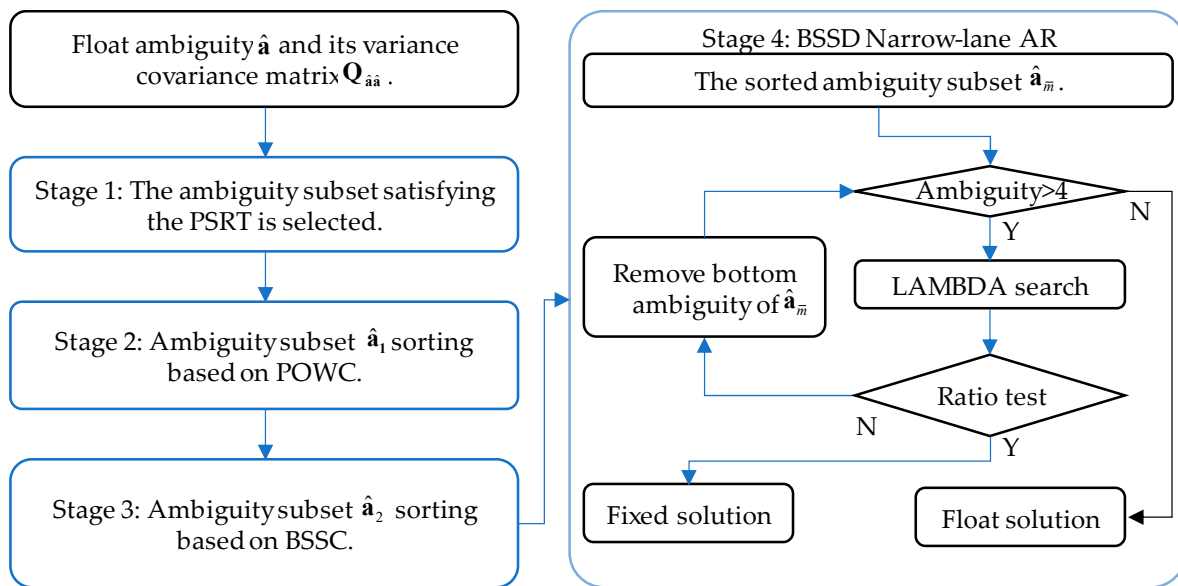


**Figure 1.** Flowchart of multi-GNSS PPP PAR method based on TSSC.

#### 4. Experiments and Analysis

To demonstrate the effectiveness of the multi-GNSS PPP PAR method based on TSSC, the static observation data from 10 MGEX stations during DOY 116–DOY 145 in 2022, and the urban kinematic data on DOY 258, 2021 were collected. The data were compared with the PAR method based on the BSSC, abbreviated as BSSC-PAR. The BSSC-PAR accepts fixed solution evaluation criteria consistent with TSSC-PAR.

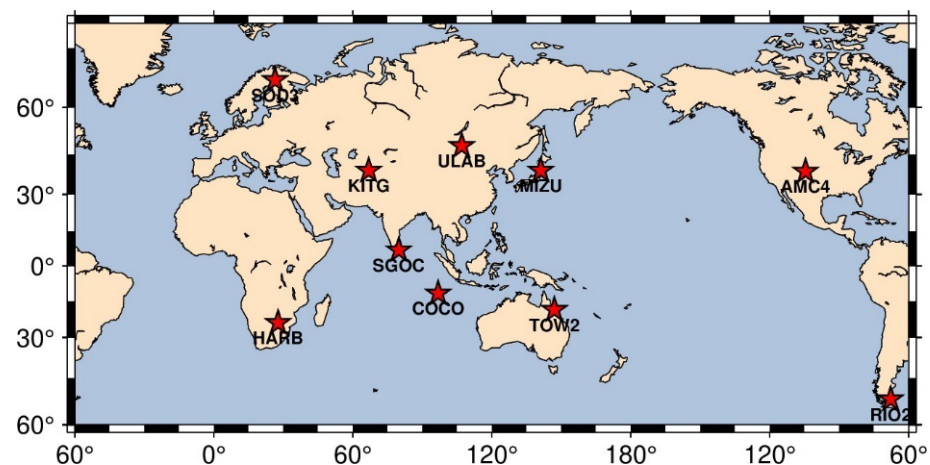
Table 1 outlines the processing strategy for the static and kinematic data. The positioning accuracy of the TSSC-PAR and BSSC-PAR shown in this paper presents fixed solutions. BDS’s Geostationary Earth Orbit (GEO) satellites are excluded from this process. This is due to the poor accuracy of their observations and orbit products. The performance of the multi-GNSS PPP PAR is evaluated, including the TTFF, positioning accuracy, and convergence time. The “true” coordinates of the stations are obtained from the IGS weekly solution file and are used as the reference for assessing positioning accuracy. The TTFF in the ambiguity-fixed solution is defined as the time to get the first correctly fixed solution, which means the ambiguity validation succeeds and positioning errors of the fixed solution are smaller than that of the float solution in the same epoch. The positioning errors are defined as the differences between positioning solutions and reference solutions. The positioning accuracy is the RMS of converged positioning errors. Convergence time is defined as the time required for a solution to achieve a horizontal positioning error of less than 10 cm and remains for at least 10 epochs.

##### 4.1. The Static Experiment

The distribution of the stations is presented in Figure 2. Due to differences in the satellite visibility from site to site, the selection of stations across the globe allows us to get a clear insight into the expected performance that is globally applicable and not location-restricted. The sampling frequency of static experimental data collected by the MGEX stations is 30 s. The static experimental data were processed using the kinematic model. To simulate PPP PAR hourly solutions, restarts were performed every hour.

**Table 1.** Data processing models and strategies of multi-GNSS PPP PAR.

Item	Strategy
Observations	IF combination of code and carrier phase
Cutoff	10°
Satellite orbit/clock errors	WHU precise orbit and carrier phase clock products ( <a href="ftp://igs.gnsswhu.cn/pub/whu/phasebias">ftp://igs.gnsswhu.cn/pub/whu/phasebias</a> , accessed on 24 February 2023)
Satellite code and carrier phase bias	WHU OSBs products
System and signal frequency	GPS: L1/L2; BDS: B1I/B3I; Galileo: E1/E5a
A priori noise	Code: 0.3 m; Carrier phase: 0.003 m
Weighting	MEO: IGSO = 1:1 [37]
Inter-system biases	$W = 1, e > 30^\circ; W = 4 \sin e^2, e < 30^\circ$ where
Tropospheric zenith hydrostatic delay	Constant
Zenith wet tropospheric delay	Saastamoinen (GPT2) [38]
Antenna phase centers	Mapping function: GMF; modeled by a random walk estimation with system noise $2.5 \times 10^{-11} \text{ m}^2/\text{s}$ [39]
IF ambiguity	igs14_2188.atx [40]
Reference satellite	Constant and random walk
Parameter estimation method	Maximum elevation angle satellite
Ambiguity resolution	Forward Kalman filter based on IGG-3
Ratio value	LAMBDA search
Minimum success rate threshold	2.0 [41]
	99.9% [13]

**Figure 2.** Station distribution map.

### The AMC4 Station Experiment

Figure 3 shows the positioning accuracy of the BSSC-PAR and TSSC-PAR for the AMC4 station in the east, north, and up directions. It can be clearly observed that the positioning accuracy of TSSC-PAR is significantly improved in the east, north, and up directions, compared with the BSSC-PAR. As shown in Table 2, the TTFF and convergence time of TSSC-PAR are 4.3 min and 7.7 min, respectively, which is an improvement of 28.3% and 18.9%, respectively, compared with the BSSC-PAR. Furthermore, the positioning error RMS of TSSC-PAR are 13.1 mm, 11.5 mm, and 42.5 mm in the east, north, and up directions, respectively, with an improvement of about 23.4%, 5.7%, and 8.2% compared with the BSSC-PAR. Figure 4 shows the number of ambiguity-fixed for the AMC4 station on the 116th day of 2022. The inaccurate variance of the ambiguity parameter due to the lower quality of the observations affects the accuracy of the ambiguity selection by the BSSC, while the TSSC-PAR uses the POWC to select a subset of ambiguities with inaccurate variances. As shown in Figure 4, during the convergence phase of the PPP, the number of ambiguity-fixed for the TSSC-PAR is higher than that for the BSSC-PAR. Combined with Figure 3 and Table 2, TSSC-PAR shows a more significant improvement in positioning performance

during the convergence phase of PPP compared with the BSSC-PAR. It means that the ambiguity subset selected by TSSC-PAR is more accurate than the one selected by BSSC-PAR. Furthermore, compared with BSSC-PAR, the average number of ambiguity-fixed for TSSC-PAR increased from 14.4 to 15.1.

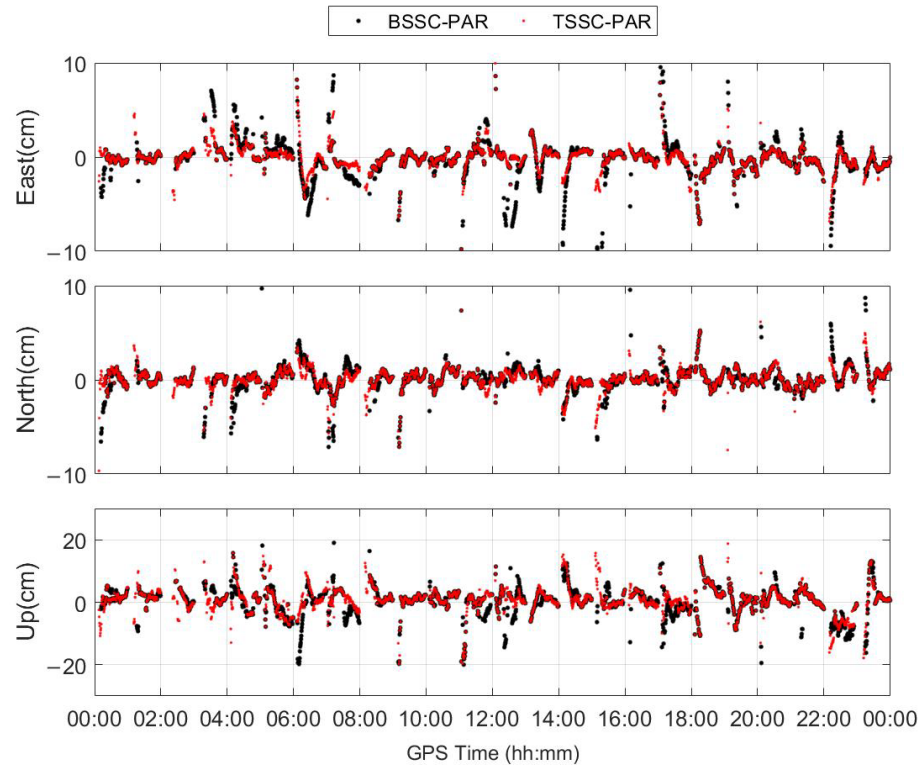


**Figure 3.** The positioning accuracy of the BSSC-PAR and TSSC-PAR for AMC4 station on DOY 116, 2022.

**Table 2.** Statistics of the TTFF, convergence time, and positioning accuracy for BSSC-PAR and TSSC-PAR for AMC4 station on DOY 116, 2022.

Solution	East (mm)	North (mm)	Up (mm)	TTFF (min)	Convergence Time (min)
BSSC-PAR	17.1	12.2	46.3	6.0	9.5
TSSC-PAR	13.1	11.5	42.5	4.3	7.7

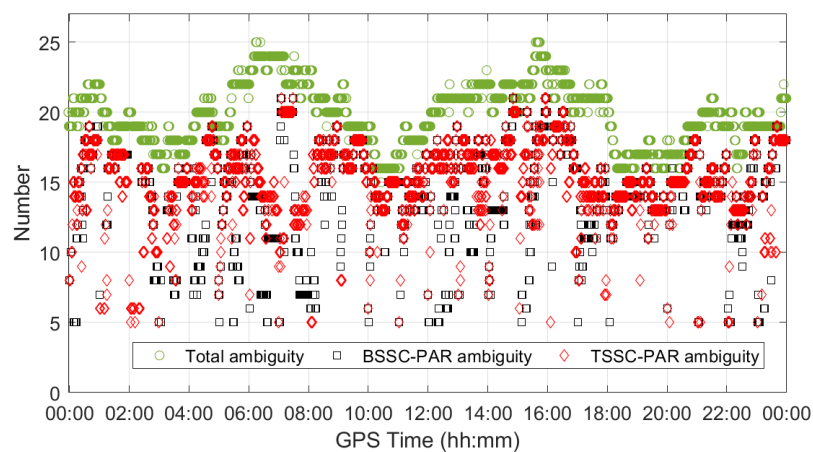


**Figure 4.** The number of ambiguity-fixed for the BSSC-PAR and TSSC-PAR for AMC4 station on DOY 116, 2022.

To further investigate the performance of the BSSC-PAR and TSSC-PAR at the AMC4 station, the data from DOY 116-DOY 145 in 2022 were analyzed. Figure 5 shows the convergence series of the BSSC-PAR and TSSC-PAR for 68% quantile in the east, north, and up directions. From Figure 5, we can see that the convergence series for the TSSC-PAR is better than that for the BSSC-PAR. Additionally, compared with the BSSC-PAR, the east convergence trend of TSSC-PAR is significantly improved. As is shown in Figure 6, the cumulative frequency of the TTFF and convergence time for the TSSC-PAR are better than the BSSC-PAR. As shown in Table 3, the RMS of positioning error for TSSC-PAR are 15.1 mm, 13.9 mm, and 47.5 mm in the east, north, and up directions, respectively. There is an improvement of 25.2%, 22.3%, and 10.8%, respectively, compared with the BSSC-PAR. Furthermore, the average TTFF and convergence time of the TSSC-PAR are 4.8 min and 7.3 min, respectively. Compared with the BSSC-PAR, the TSSC-PAR has an improvement of 11.1% and 21.5%, respectively. Figure 7 shows the distribution of the ambiguities-fixed number for BSSC-PAR and TSSC-PAR. From Figure 7, we can see that the distribution of the ambiguity-fixed number for TSSC-PAR is better than that for BSSC-PAR. Combined with Figures 5 and 6 and Table 3, with the increase of the ambiguity-fixed number, the positioning performance of the TSSC-PAR is better than the BSSC-PAR. Based on the multiday data in the AMC4 station, it can be concluded that the TTFF, convergence time, and positioning accuracy of the TSSC-PAR are superior to that of the BSSC-PAR.

**Table 3.** The statistics of the TTFF, convergence time, and positioning accuracy for BSSC-PAR and TSSC-PAR for AMC4 station DOY 116 to DOY 145, 2022.

Solution	East (mm)	North (mm)	Up (mm)	TTFF (min)	Convergence Time (min)
BSSC-PAR	20.2	17.9	53.3	5.4	9.3
TSSC-PAR	15.1	13.9	47.5	4.8	7.3

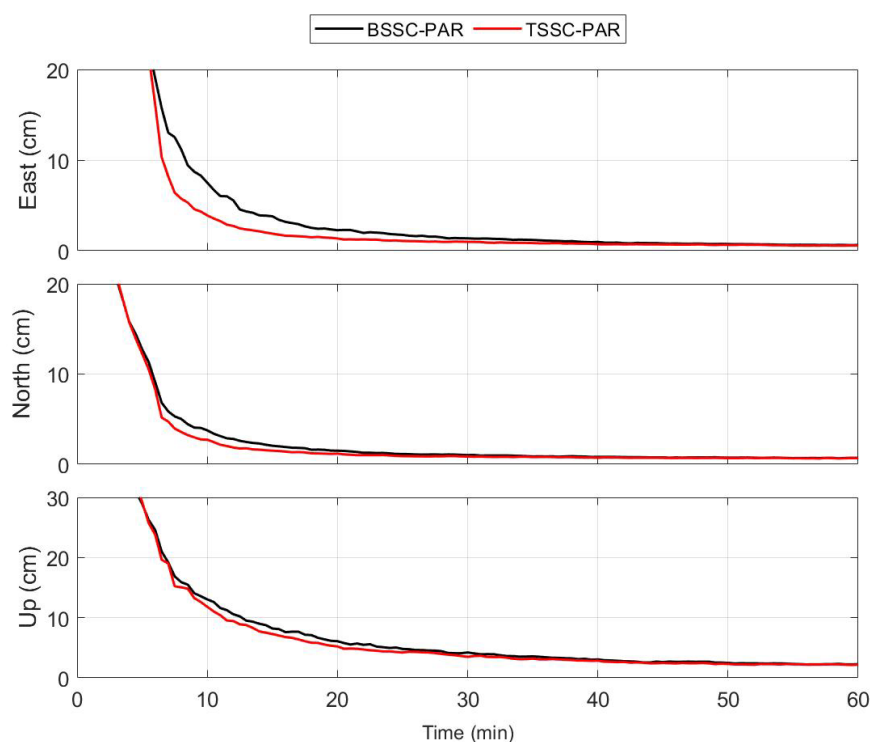


**Figure 5.** Convergence series of the BSSC-PAR and TSSC-PAR for 68% quantile of the east, north, and up in 1 h pass.

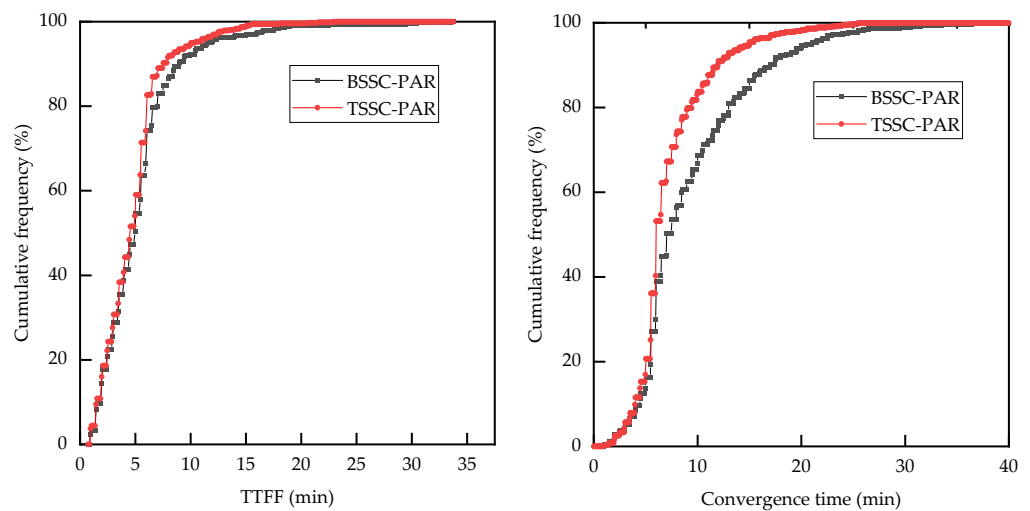


**Figure 6.** Cumulative frequency of the TTF and convergence time for BSSC-PAR and TSSC-PAR for AMC4 station DOY 116 to DOY 145, 2022.

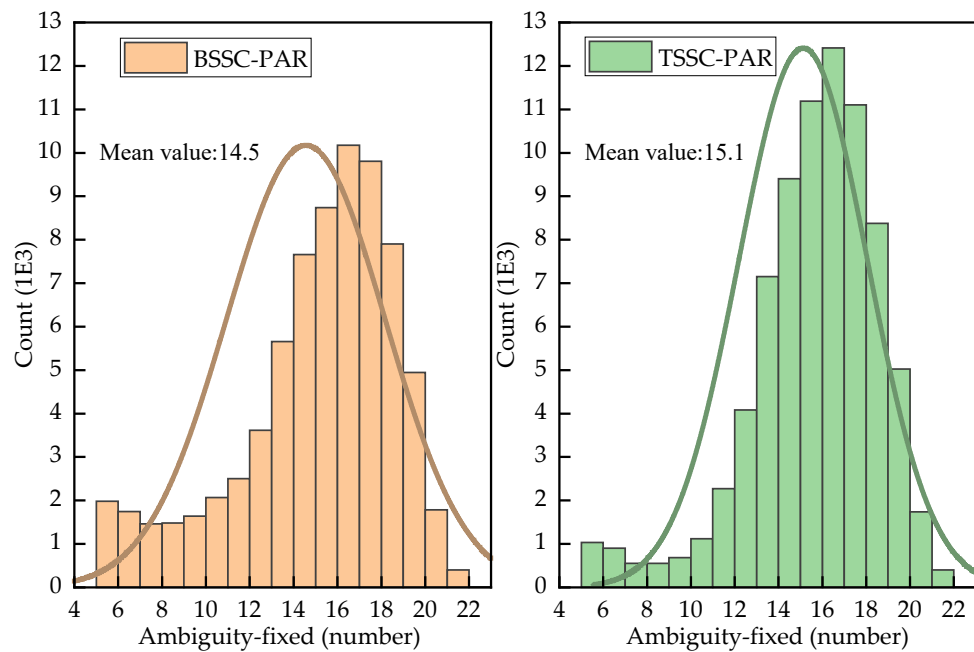


**Figure 7.** Distribution of ambiguity-fixed number for BSSC-PAR and TSSC-PAR for AMC4 station DOY 116 to DOY 145, 2022.4.1.2. The Multi-Station Experiment.

In order to assess the global applicability of the TSSC-PAR performance, static data from 10 MGEX stations were analyzed. Figure 8 shows the RMS of positioning error for BSSC-PAR and TSSC-PAR in the east, north, and up directions. The positioning accuracy for the TSSC-PAR is better than that for the BSSC-PAR at each station as shown in Figure 8. In Figure 9, the TTF and convergence time for the TSSC-PAR are better than that for the BSSC-PAR. Table 4 gives the statistic indicators of the BSSC-PAR and TSSC-PAR. Compared with the BSSC-PAR, the positioning accuracy of the TSSC-PAR has improved by 20.1%, 17.1%, and 4.67%, and it has eventually reached 20.7 mm, 14.8 mm, and 58.8 mm in the east, north, and up directions, respectively. Furthermore, compared with the BSSC-PAR, the average TTF and convergence time for the TSSC-PAR are 3.15 min and 5.2 min, which is an improvement of 8.7% and 16.8%, respectively. As shown in Figure 10, the distribution of the ambiguity-fixed number for the TSSC-PAR is better than that for the BSSC-PAR. The average number of the ambiguity-fixed solutions for TSSC-PAR and BSSC-PAR are 17.0 and

16.1, respectively. Therefore, compared with the BSSC-PAR, the ambiguity subset selected by the TSSC-PAR is more accurate. To sum up, the positioning performance of TSSC-PAR is still better than that of BSSC-PAR under the verification of large amounts of static data.

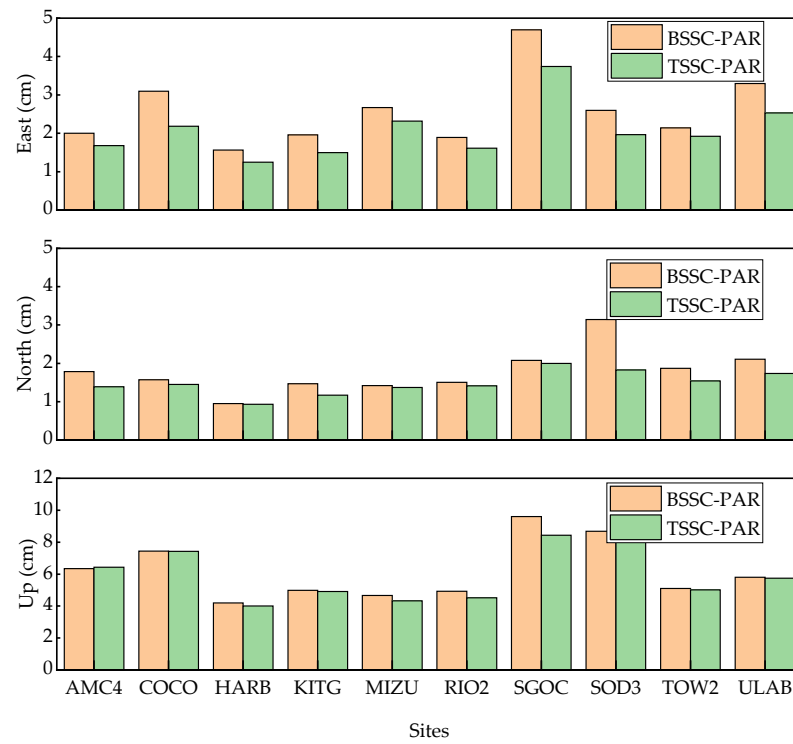


Figure 8. The positioning accuracy of the east, north, and up for the BSSC-PAR and TSSC-PAR.

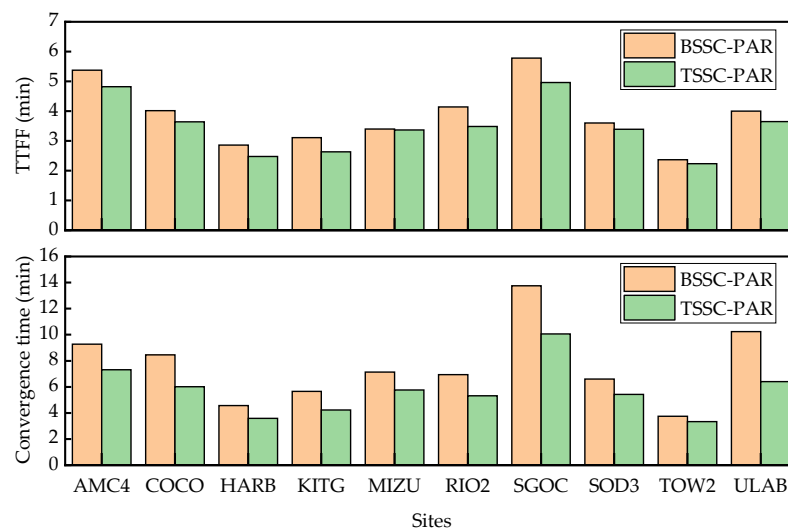
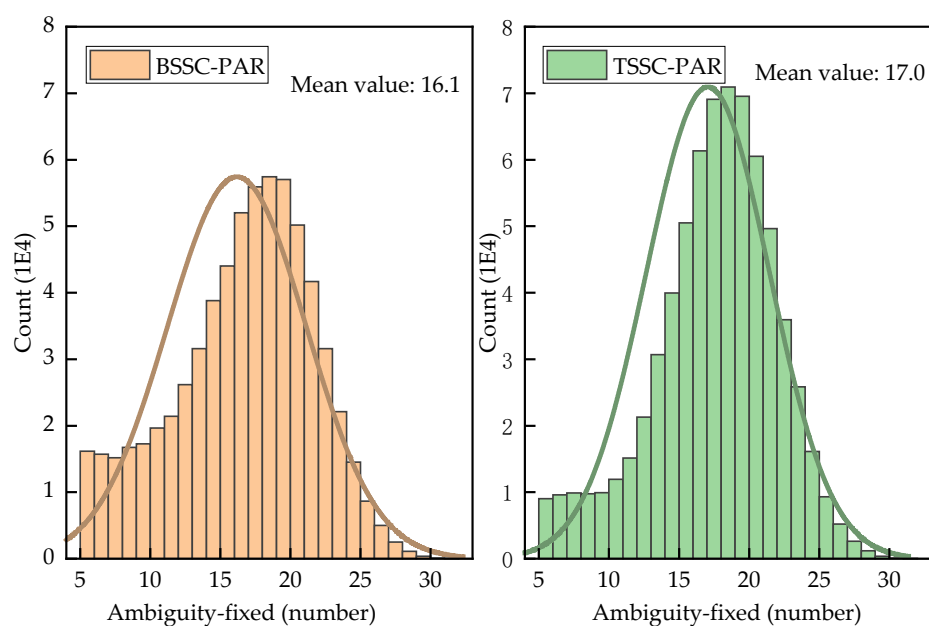


Figure 9. The average TTF and average convergence time for the BSSC-PAR and TSSC-PAR.

Table 4. Statistics of TTF, convergence time, and positioning accuracy of the BSSC-PAR and TSSC-PAR.

Solution	East (mm)	North (mm)	Up (mm)	TTF (min)	Convergence Time (min)
BSSC-PAR	17.1	12.2	46.3	3.45	6.25
TSSC-PAR	13.1	11.5	42.5	3.15	5.2



**Figure 10.** Distribution of ambiguity-fixed number for the BSSC-PAR and TSSC-PAR for selection stations from DOY 116 to DOY 145, 2022.

#### 4.2. The Kinematic Experiment

Table 5 summarizes the basic information from kinematic experiments. Figure 11 shows the reference station position and vehicle trajectory, where the longest baseline between the reference station and the vehicle is 2 km. RTK can obtain centimeter-level or even millimeter-level positioning accuracy. Therefore, we use fixed solution RTK of BDS/GPS combination by RTKLIB software as the reference true value, which is used to evaluate the performance of the TSSC-PAR and BSSC-PAR.

**Table 5.** Basic information of the experiment in urban areas.

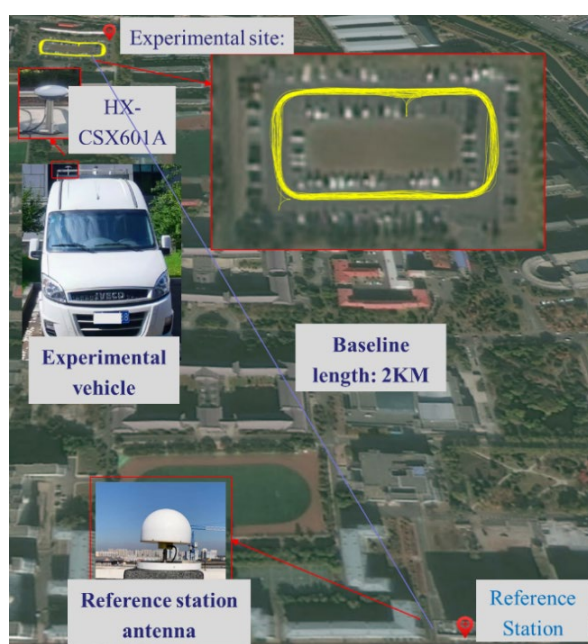
Experiment	Information
Starting time	2021, 258, GPS time 04:58:45
Ending time	2021, 258, GPS time 06:05:39
Sampling interval (s)	1
Base station receiver	OEM628E
Base station antenna	Novatel 750
Rover station receiver	OEM729
Rover station antenna	Harxon HX-CSX601A

Figure 12 shows the value of the PDOP and HDOP of the kinematic experiment. From Figure 12, we can see that the value of the PDOP and HDOP varies rapidly. Figure 13 shows that the positioning accuracy of the TSSC-PAR is significantly better than that of the BSSC-PAR, in the east, north, and up directions. Figure 14 shows the number of ambiguity-fixed solutions for the BSSC-PAR and TSSC-PAR. Compared with the BSSC-PAR, the average number of ambiguity-fixed solutions for the TSSC-PAR increased from 12.9 to 13.6. Combined with Figures 13 and 14, it can be seen that the number of ambiguity-fixed solutions by the TSSC-PAR is better than that by the BSSC-PAR in the PPP initialization phase. The positioning accuracy of the TSSC-PAR is better than that of the BSSC-PAR in the PPP initialization phase. Although there is little difference in the TTFF between the TSSC-PAR and BSSC-PAR, the convergence time of TSSC-PAR is significantly shorter than that of the BSSC-PAR. Table 6 gives the statistic indicators of the kinematic experiment for the BSSC-PAR and TSSC-PAR. The results are evaluated, including positioning accuracy, TTFF, and convergence time. Compared with BSSC-PAR, the positioning accuracy of TSSC-

PAR improved by 38.1%, 1.4%, and 2.2% in the east, north, and up directions, respectively. Additionally, the TTFF and convergence time decreased from 1.65 min and 10.5 min to 1.3 min and 1.8 min, respectively. In conclusion, the experimental results have demonstrated that the TSSC-PAR has a better performance than the BSSC-PAR in kinematic scenes.

**Table 6.** Statistics of TTFF, convergence time, and positioning accuracy of the BSSC-PAR and TSSC-PAR in the kinematic experiment.

Solution	East (mm)	North (mm)	Up (mm)	TTFF (min)	Convergence Time (min)
BSSC-PAR	65.2	42.7	27.3	1.65	10.5
TSSC-PAR	40.3	42.1	26.7	1.3	1.8



**Figure 11.** Reference station position and vehicle tracking in the kinematic experiment.

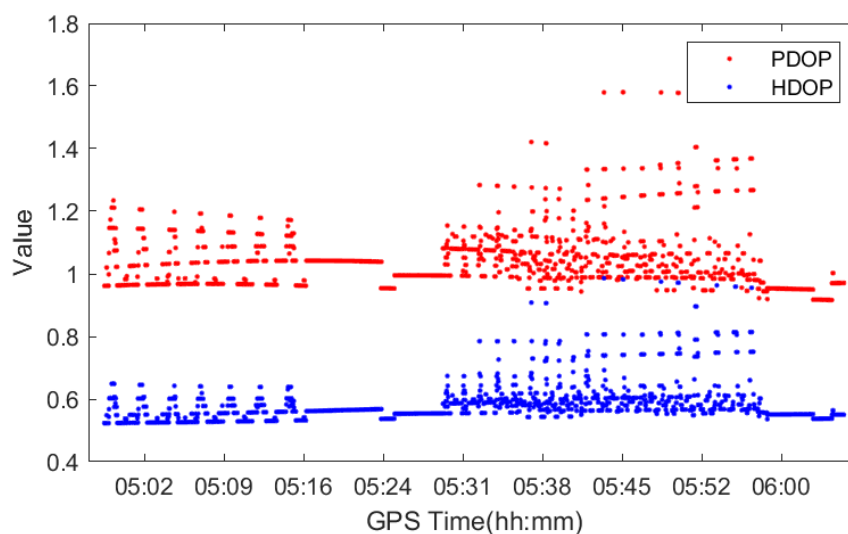


**Figure 12.** PDOP (red) and HDOP (blue) of the kinematic experiment.

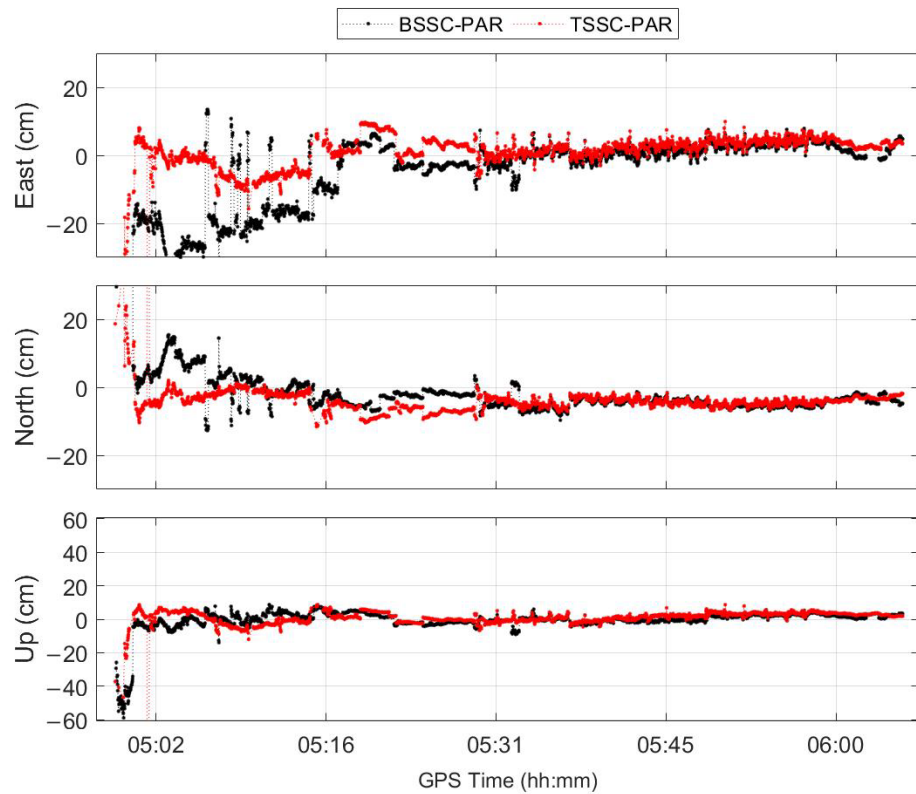


Figure 13. The positioning accuracy of the BSSC-PAR and TSSC-PAR in the kinematic experiment.

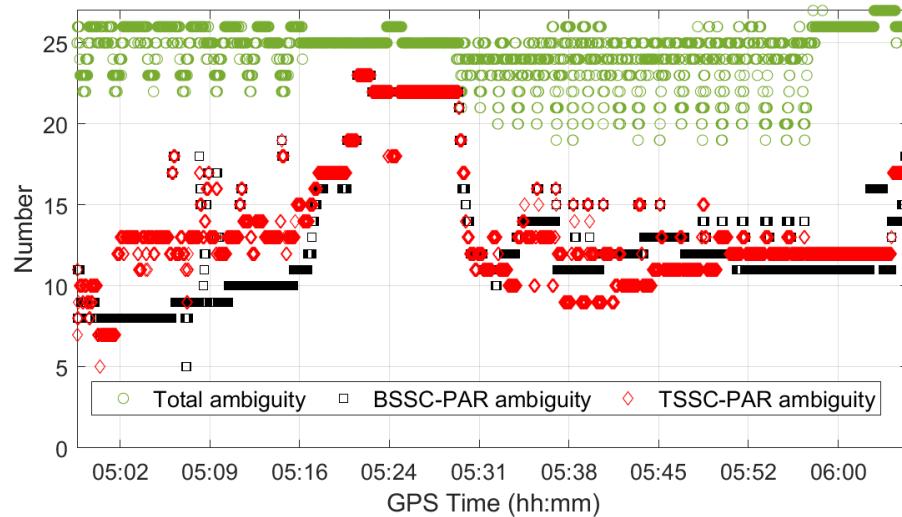


Figure 14. The number of ambiguity-fixed for the BSSC-PAR and TSSC-PAR in the kinematic experiment.

### 5. Discussion

The PAR can enhance the AR success rate and reduce the TTFF. The core of PAR is the selection of the ambiguity subset. In this study, we aim to address the influence of inaccurate variance of ambiguity parameters, particularly those with low observation quality, on the ambiguity subset selection based on the BSSC. In this contribution, the observations whose elevation angle is below  $30^\circ$  or whose posterior residual falls into the IGG3 model reduction domain are clustered together. The POWC instead of the BSSC is adopted to sort ambiguities to overcome the false convergence of variance. In static and kinematic experiments and analysis, we can see that the performance of the TSSC-PAR is better than that of the BSSC-PAR.

The present study evaluates kinematic performance using limited real data; future research will involve additional kinematic experiments conducted in various urban environments. Furthermore, the method presented in this paper conducts post-processing analysis with fast precise ephemeris. Future research will focus on multi-GNSS real-time PPP PAR. Due to the potential influence on the accuracy of real-time satellite clock and orbit service, experimental verification is necessary to confirm the effectiveness of low-precision ambiguity screening in real-time PPP PAR. We hope that future research will leverage the multi-GNSS PPP PAR method based on the two-step sorting criterion to further shorten convergence time in real-time data and enhance the practicality of the proposed method.

## 6. Conclusions

The selection criterion for the ambiguity subset is crucial for improving the positioning performance of PAR. To avoid the adverse effects of ambiguity variance inaccuracy on the PAR when using the BSSC, we proposed an improved multi-GNSS PPP PAR method based on the TSSC. The observation data from 10 stations in the MGEX during the period from DOY 116 to DOY 145 in 2022, along with urban kinematic data from DOY 258 in 2021, were used to verify the performance of the proposed method.

The static experiment results demonstrate that the probability distribution of the ambiguity-fixed number for the TSSC-PAR is better than that for the BSSC-PAR. Compared with the BSSC-PAR, the positioning accuracy improved by 20.1%, 17.1%, and 4.67% in the east, north, and up directions, respectively. The average TTFF and convergence time improved by 8.7% and 16.8%, respectively. Compared with the BSSC-PAR, the urban kinematic experiment results demonstrate that the positioning accuracy for the TSSC-PAR enhanced by 38.1%, 1.4%, and 2.2%, in the east, north, and up directions, respectively. The TTFF and convergence time decreased from 1.65 min and 10.5 min to 1.3 min and 1.8 min, respectively. In summary, the positioning performance of the TSSC-PAR is better than that of the BSSC-PAR for static and kinematic data.

**Author Contributions:** Conceptualization, L.Z. and Z.S.; methodology, L.Z. and Z.S.; software, Z.S. and F.Y.; validation, L.Z., Z.S., F.Y. and X.L.; formal analysis, Z.S.; investigation, Z.S., F.Y. and J.Z.; resources, X.L. and J.Z. All authors have read and agreed to the published version of the manuscript.

**Funding:** This research was jointly funded by the National Key Research and Development Program (No. 2021YFB3901300), the National Natural Science Foundation of China (Nos. 62003109, 61773132, 61633008, 61803115), the 145 High-Tech Ship Innovation Project sponsored by the Chinese Ministry of Industry and Information Technology, the Heilongjiang Province Research Science Fund for Excellent Young Scholars (No. YQ2020F009), and the Fundamental Research Funds for Central Universities (Nos. 3072019CF0401, 3072020CFT0403).

**Data Availability Statement:** The GNSS data and IGS SINEX weekly solutions files are by (<https://cddis.nasa.gov/archive/gps/data/daily>, accessed on 1 February 2023). The precise ephemerides and OSB product provided by Wuhan University are available at (<ftp://igs.gnsswhu.cn/pub/whu>, accessed on 24 February 2023). The kinematic data are not applicable.

**Acknowledgments:** All authors gratefully acknowledge WHU and IGS for providing the data, orbit, and clock products.

**Conflicts of Interest:** The authors declare no conflict of interest.

## References

1. Zumberge, J.F.; Heflin, M.B.; Jefferson, D.C.; Watkins, M.M.; Webb, F.H. Precise point positioning for the efficient and robust analysis of GPS data from large networks. *J. Geophys. Res. Solid. Earth* **1997**, *102*, 5005–5017. [[CrossRef](#)]
2. Ge, M.; Gendt, G.; Rothacher, M.; Shi, C.; Liu, J. Resolution of GPS carrier-phase ambiguities in Precise Point Positioning (PPP) with daily observations. *J. Geod.* **2008**, *82*, 389–399. [[CrossRef](#)]
3. Laurichesse, D.; Mercier, F.; Berthias, J.P.; Broca, P.; Cerri, L. Integer Ambiguity Resolution on Undifferenced GPS Phase Measurements and Its Application to PPP and Satellite Precise Orbit Determination. *Annu. Navig.* **2009**, *56*, 135–149. [[CrossRef](#)]
4. Collins, P.; Bisnath, S.; Lahaye, F.; Héroux, P. Undifferenced GPS Ambiguity Resolution Using the Decoupled Clock Model and Ambiguity Datum Fixing. *Annu. Navig.* **2010**, *57*, 123–135. [[CrossRef](#)]

5. Psychas, D.; Verhagen, S.; Teunissen, P.J.G. Precision analysis of partial ambiguity resolution-enabled PPP using multi-GNSS and multi-frequency signals. *Adv. Space Res.* **2020**, *66*, 2075–2093. [[CrossRef](#)]
6. Li, X.; Ge, M.; Zhang, H.; Wickert, J. A method for improving uncalibrated phase delay estimation and ambiguity-fixing in real-time precise point positioning. *J. Geod.* **2013**, *87*, 405–416. [[CrossRef](#)]
7. Geng, J.; Meng, X.; Dodson, A.; Teferle, N. Integer ambiguity resolution in precise point positioning: Method comparison. *J. Geod.* **2010**, *84*, 569–581. [[CrossRef](#)]
8. Zhao, Q.; Guo, J.; Liu, S.; Tao, J.; Hu, Z.; Chen, G. A variant of raw observation approach for BDS/GNSS precise point positioning with fast integer ambiguity resolution. *Satell. Navig.* **2021**, *2*, 29. [[CrossRef](#)]
9. Li, X.; Ge, M.; Dai, X.; Ren, X.; Fritsche, M.; Wickert, J.; Schuh, H. Accuracy and reliability of multi-GNSS real-time precise positioning: GPS, GLONASS, BeiDou, and Galileo. *J. Geod.* **2015**, *89*, 607–635. [[CrossRef](#)]
10. Yang, F.; Zheng, C.; Zhang, J.; Sun, Z.; Li, L.; Zhao, L. The Initial Performance Evaluation of Mixed Multi-Frequency Undifferenced and Uncombined BDS-2/3 Precise Point Positioning under Urban Environmental Conditions. *Remote Sens.* **2022**, *14*, 5525. [[CrossRef](#)]
11. Zhang, J.; Zhao, L.; Yang, F.; Li, L.; Liu, X.; Zhang, R. Integrity monitoring for undifferenced and uncombined PPP under the local environment. *Meas. Sci. Technol.* **2022**, *33*, 065010. [[CrossRef](#)]
12. Li, P.; Zhang, X. Precise Point Positioning with Partial Ambiguity Fixing. *Sensors* **2015**, *15*, 13627–13643. [[CrossRef](#)] [[PubMed](#)]
13. Teunissen, P.J.G. Success probability of integer GPS ambiguity rounding and bootstrapping. *J. Geod.* **1998**, *72*, 606–612. [[CrossRef](#)]
14. Mowlam, A. Baseline Precision Results Using Triple Frequency Partial Ambiguity Sets. In Proceedings of the 17th International Technical Meeting of the Satellite Division of the Institute of Navigation, ION GNSS 2004, Long Beach, CA, USA, 21–24 September 2004; Institute of Navigation: Long Beach, CA, USA, 2004; pp. 2509–2518.
15. Teunissen, P. Integer Aperture GNSS Ambiguity Resolution. *Artif. Satell.* **2003**, *38*, 79–88.
16. Teunissen, P.; Verhagen, S. The GNSS Ambiguity Ratio-test Revisited: A Better Way of Using it. *Surv. Rev.* **2009**, *41*, 138–151. [[CrossRef](#)]
17. Teunissen, P.; Verhagen, S. Integer Aperture Estimation—A Framework for GNSS Ambiguity Acceptance Testing. *Inside GNSS* **2011**, *2011*, 66–73.
18. Li, L.; Shi, H.; Jia, C.; Cheng, J.; Li, H.; Zhao, L. Position-domain integrity risk-based ambiguity validation for the integer bootstrap estimator. *GPS Solut.* **2018**, *22*, 39. [[CrossRef](#)]
19. Wang, J.; Feng, Y. Reliability of partial ambiguity fixing with multiple GNSS constellations. *J. Geod.* **2013**, *87*, 3. [[CrossRef](#)]
20. Li, B.; Shen, Y.; Feng, Y.; Gao, W.; Yang, L. GNSS ambiguity resolution with controllable failure rate for long baseline network RTK. *J. Geod.* **2014**, *88*, 99–112. [[CrossRef](#)]
21. Li, Z.; Xu, G.L.; Guo, J.; Zhao, Q.L. A sequential ambiguity selection strategy for partial ambiguity resolution during RTK positioning in urban areas. *GPS Solut.* **2022**, *26*, 92. [[CrossRef](#)]
22. Gendt, G.; Dick, G.; Reigber, C.; Tomassini, M.; Liu, Y. Demonstration of NRT GPS water vapor monitoring for numerical weather prediction in Germany. *J. Meteorol. Soc. Jpn.* **2004**, *82*, 361–370. [[CrossRef](#)]
23. Geng, J.; Chen, X.; Pan, Y.; Mao, S.; Zhang, K. PRIDE PPP-AR: An open-source software for GPS PPP ambiguity resolution. *GPS Solut.* **2019**, *23*, 91. [[CrossRef](#)]
24. Sun, Z.; Zhao, L.; Yang, F.; Zhang, J.; Zhang, R. A Multi-GNSS PPP Partial Ambiguity Resolution Method Based on Observations Weight Ranking. In Proceedings of the 2023 International Technical Meeting of The Institute of Navigation, Long Beach, CA, USA, 22–25 January 2023; pp. 624–636.
25. Henkel, P.; Günther, C. Partial integer decorrelation: Optimum trade-off between variance reduction and bias amplification. *J. Geod.* **2010**, *84*, 51–63. [[CrossRef](#)]
26. Gao, W.; Gao, C.; Pan, S. A method of GPS/BDS/GLONASS combined RTK positioning for middle-long baseline with partial ambiguity resolution. *Surv. Rev.* **2015**, *49*, 1752270615Y.000. [[CrossRef](#)]
27. Tabaček, J.; Havlena, V. Schmidt-Kalman Filters for Systems with Uncertain Parameters and Asynchronous Sampling. In Proceedings of the 2018 18th International Conference on Control, Automation and Systems (ICCAS), PyeongChang, Republic of Korea, 17–20 October 2018; pp. 357–362.
28. Zanetti, R.; D’Souza, C. Recursive Implementations of the Schmidt-Kalman ‘Consider’ Filter. *J. Astronaut. Sci.* **2013**, *60*, 672–685. [[CrossRef](#)]
29. Kouba, J.; Héroux, P. Precise Point Positioning Using IGS Orbit and Clock Products. *GPS Solut.* **2001**, *5*, 12–28. [[CrossRef](#)]
30. Villiger, A.; Schaer, S.; Dach, R.; Prange, L.; Sušnik, A.; Jäggi, A. Determination of GNSS pseudo-absolute code biases and their long-term combination. *J. Geod.* **2019**, *93*, 1487–1500. [[CrossRef](#)]
31. Schaer, S. Bias-SINEX Format and Implications for IGS Bias Products. IGS Workshop 2018. Available online: [https://files.igs.org/pub/data/format/sinex\\_bias\\_100.pdf](https://files.igs.org/pub/data/format/sinex_bias_100.pdf) (accessed on 24 February 2023).
32. Hatch, R.R. The Synergism of GPS Code and Carrier Measurements. *Int. Geod. Symp. Satell. Doppler Position* **1982**, *2*, 1213–1231.
33. Melbourne, W.G. The case for ranging in GPS-based geodetic systems. In Proceedings of the First International Symposium on Precise Positioning with the Global Positioning System, Rockville, MD, USA, 15–19 April 1985; US Department of Commerce: Rockville, MD, USA, 1985; pp. 373–386.

34. Wübbena, G. Software developments for geodetic positioning with GPS using TI 4100 code and carrier measurements. In Proceedings of the First International Symposium on Precise Positioning with the Global Positioning System, Rockville, MD, USA, 15–19 April 1985; US Department of Commerce: Rockville, MD, USA, 1985; pp. 403–412.
35. Yang, Y.; Song, L.; Xu, T. Robust estimator for correlated observations based on bifactor equivalent weights. *J. Geod.* **2002**, *76*, 353–358. [[CrossRef](#)]
36. Yang, F.; Zhao, L.; Li, L.; Feng, S.; Cheng, J. Performance Evaluation of Kinematic BDS/GNSS Real-Time Precise Point Positioning for Maritime Positioning. *J. Navig.* **2019**, *72*, 34–52. [[CrossRef](#)]
37. Shu, B.; Liu, H.; Wang, L.; Huang, G.; Zhang, Q.; Yang, Z. Performance improvement of real-time PPP ambiguity resolution using a regional integer clock. *Adv. Space Res.* **2021**, *67*, 1623–1637. [[CrossRef](#)]
38. Böhm, J.; Möller, G.; Schindelegger, M.; Pain, G.; Weber, R. Development of an improved empirical model for slant delays in the troposphere (GPT2w). *GPS Solut.* **2015**, *19*, 433–441. [[CrossRef](#)]
39. Liu, T.; Chen, H.; Chen, Q.; Jiang, W.; Laurichesse, D.; An, X.; Geng, T. Characteristics of phase bias from CNES and its application in multi-frequency and multi-GNSS precise point positioning with ambiguity resolution. *GPS Solut.* **2021**, *25*, 58. [[CrossRef](#)]
40. Loyer, S.; Banville, S.; Geng, J.; Strasser, S. Exchanging satellite attitude quaternions for improved GNSS data processing consistency. *Adv. Space Res.* **2021**, *68*, 2441–2452. [[CrossRef](#)]
41. Leick, A.; Rapoport, L.; Tatarnikov, D. *GPS Satellite Surveying*; John Wiley & Sons, Inc.: Hoboken, NJ, USA, 2015.

**Disclaimer/Publisher’s Note:** The statements, opinions and data contained in all publications are solely those of the individual author(s) and contributor(s) and not of MDPI and/or the editor(s). MDPI and/or the editor(s) disclaim responsibility for any injury to people or property resulting from any ideas, methods, instructions or products referred to in the content.